CALPHAD: Computer Coupling of Phase Diagrams and Thermochemistry 68 (2020) 101734

Contents lists available at ScienceDirect

Calphad

journal homepage: http://www.elsevier.com/locate/calphad

The phase equilibria of the Cu–Cr–Ni and Cu–Cr–Ag systems: Experimental investigation and thermodynamic modeling

Chengliang Qiu [a], Biao Hu [a,*], Jiaqiang Zhou [a], Peilu Wu [a], Yin Liu [a], Chengjun Wang [b], Yong Du [c]

[a] School of Materials Science and Engineering, Anhui University of Science and Technology, Huainan, Anhuim, 232001, PR China
[b] State Key Laboratory of Mining Response and Disaster Prevention and Control in Deep Coal Mines, Anhui University of Science and Technology, Huainan, Anhui, 232001, PR China
[c] State Key Laboratory of Powder Metallurgy, Central South University, Changsha, Hunan, 410083, PR China

ARTICLE INFO

Keywords:
Cu–Cr–Ni system
Cu–Cr–Ag system
Phase equilibria
Thermodynamic modeling
Experimental investigation

ABSTRACT

The phase equilibria of the Cu–Cr–Ni and Cu–Cr–Ag systems were investigated by a combination of key experiments and thermodynamic modeling. Eleven and fourteen ternary alloys were prepared to determine the isothermal sections of the Cu–Cr–Ni system at 800 and 1000 °C, and the Cu–Cr–Ag system at 500, 600, 650 and 700 °C, respectively, by means of X-ray diffraction (XRD) and scanning electron microscopy with energy dispersive X-ray spectroscopy (SEM/EDX). The three- and two-phase regions were determined. The solubility of the third elements in the phases of the binary systems was measured. No ternary compound was found in these two ternary systems. Based on the experimental equilibria data from the literature and the present work, a thermodynamic modeling of the Cu–Cr–Ni and Cu–Cr–Ag systems was performed by the CALPHAD (CALculation of PHAse Diagrams) method. The substitutional solution model was used to describe the solution phases. A set of self-consistent thermodynamic parameters of the Cu–Cr–Ni and Cu–Cr–Ag systems was obtained. Most of the reliable experimental data can be well reproduced by the present thermodynamic modeling.

1. Introduction

Copper alloys are widely used in electricity, electron communication, aerospace, transportation and other fields due to their high electrical conductivity, high thermal conductivity, good mechanical properties, good corrosion resistance, etc. [1–3]. The high electrical conductivity and high thermal conductivity are the most important characteristics of copper. However, the strength of pure copper is low, which can be improved by adding alloy elements, such as Cr, Ni, Ag. Cu–Cr based alloys are the high strength and high conductivity copper alloys and have been widely studied [4–10]. Cu and Ni can form the infinite solid solution and Ni can improve the strength, corrosion resistance and thermoelectricity of copper [11]. The addition of Ag significantly can improve strength, stress relaxation resistance and bend formability of copper [12]. The design of new high strength and high conductivity copper alloy requires information about the phase equilibria and thermodynamic properties of the Cu–Cr based ternary systems. Therefore, a thorough thermodynamic assessment of the Cu–Cr–Ni and Cu–Cr–Ag systems is necessary for providing a set of reliable thermodynamic parameters for thermodynamic extrapolations to related higher order systems.

The phase equilibria of the ternary Cu–Cr–Ni system have been studied by several groups of researchers [13–16]. The isothermal section of the Cu–Cr–Ni system at 930 °C was investigated by Meijering et al. [13] by means of XRD method. One three-phase region fcc(Cu) + fcc (Cr) + bcc(Ni) and two two-phase regions fcc(Cu) + fcc(Ni) and fcc(Cu) + bcc(Cr) were determined. Subsequently, Meijering [14] tentatively calculated the 930 °C isothermal section of the Cu–Cr–Ni system using the regular approximation. The results showed that quantitative agreement between the calculated isothermal section and experimental data was poor. In 2006, the isothermal sections of the Cu–Cr–Ni system at 800 and 1000 °C were investigated by Ikoma [15]. The three- and two-phase regions were determined by means of XRD and SEM/EDX. Then Ikoma and Kajihara [16] thermodynamically assessed the Cu–Cr–Ni system based on their own experiment data [15]. The calculated results were in agreement with the experimental data [15]. However, the thermodynamic parameters of the binary systems of the Cu–Cr–Ni system accepted by Ikoma and Kajihara [16] are inconsistent with the ones in

* Corresponding author.
E-mail addresses: hubiao05047071@163.com, bhu@aust.edu.cn (B. Hu).

https://doi.org/10.1016/j.calphad.2019.101734
Received 9 September 2019; Received in revised form 23 December 2019; Accepted 24 December 2019
Available online 5 January 2020

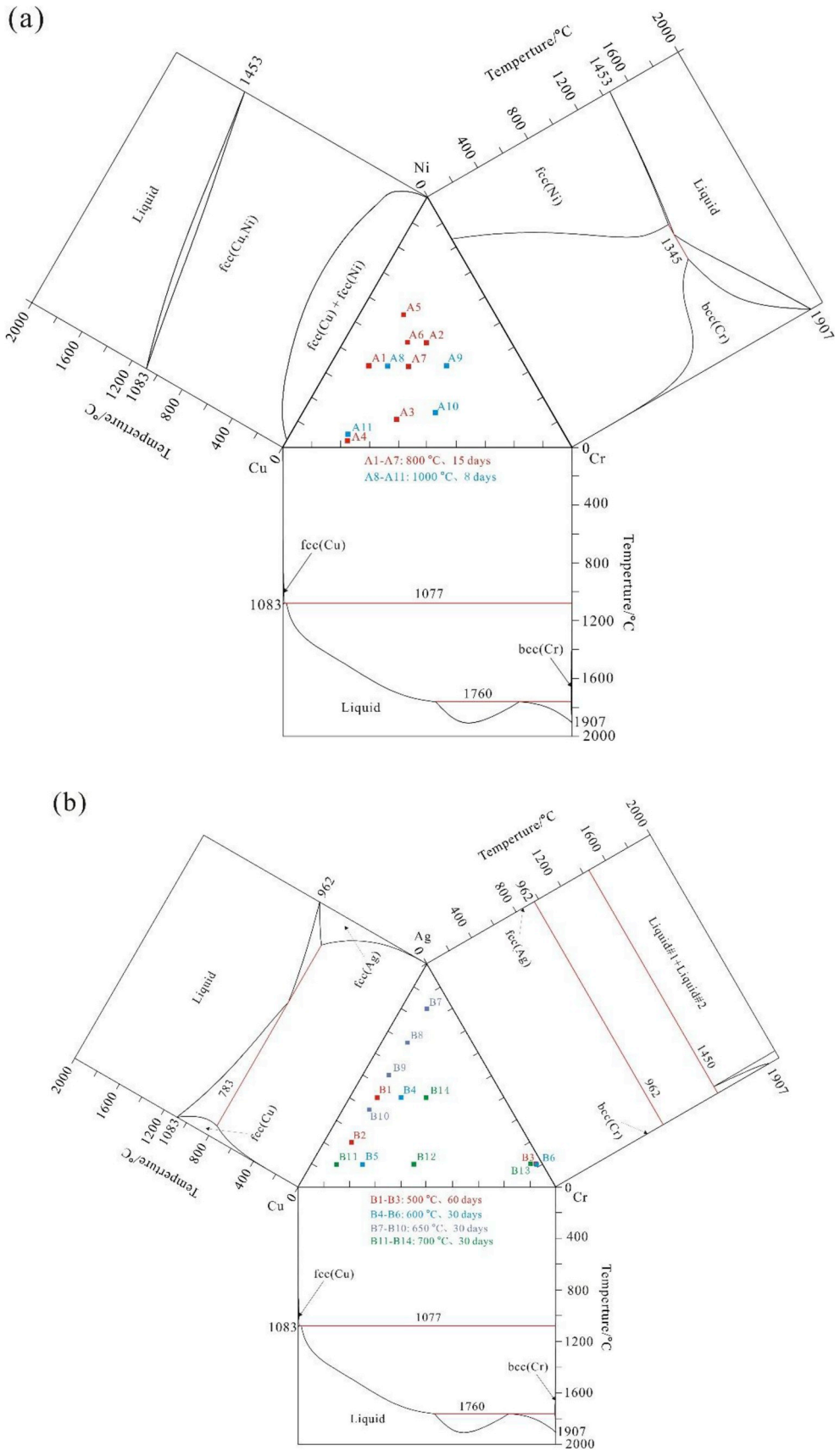

Fig. 1. Binary phase diagrams [24–28] and nominal compositions of alloys in (a) Cu–Cr–Ni and (b) Cu–Cr–Ag ternary systems.

Table 1
Phases and compositions of the Cu–Cr–Ni alloys annealed at 800 and 1000 °C.

Alloy No.	Nominal composition (at. %)	Annealed time (days)	Annealed temperature (°C)	Phases identified by XRD and SEM/EDX	Composition (at. %)		
					Cu	Cr	Ni
A1	$Cu_{54.15}Cr_{13.47}Ni_{32.38}$	15	800	fcc(Cu)	80.82	2.30	16.88
				fcc(Ni)	14.03	30.49	55.48
A2	$Cu_{29.15}Cr_{29.08}Ni_{41.77}$	15	800	fcc(Cu)	80.50	3.37	16.13
				fcc(Ni)	9.23	33.32	57.45
				bcc(Cr)	2.52	93.54	3.94
A3	$Cu_{55.79}Cr_{33.52}Ni_{10.69}$	15	800	fcc(Cu)	82.77	2.03	15.20
				bcc(Cr)	2.75	92.15	5.10
A4	$Cu_{76.97}Cr_{20.58}Ni_{2.45}$	15	800	fcc(Cu)	93.99	1.78	4.23
				bcc(Cr)	3.96	94.75	1.29
A5	$Cu_{31.50}Cr_{15.70}Ni_{52.80}$	20	800	fcc(Cu)	66.73	3.96	29.31
				fcc(Ni)	16.88	18.04	65.08
A6	$Cu_{36.40}Cr_{21.80}Ni_{41.80}$	20	800	fcc(Cu)	79.46	3.67	16.87
				fcc(Ni)	11.19	32.32	56.49
A7	$Cu_{40.70}Cr_{26.80}Ni_{32.50}$	20	800	fcc(Cu)	78.45	4.14	17.41
				fcc(Ni)	12.08	32.49	55.43
				bcc(Cr)	2.93	94.55	2.52
A8	$Cu_{47.35}Cr_{20.29}Ni_{32.36}$	8	1000	fcc(Cu)	75.23	5.65	19.12
				fcc(Ni)	13.75	35.73	50.52
A9	$Cu_{27.06}Cr_{40.57}Ni_{32.37}$	8	1000	fcc(Cu)	68.85	9.63	21.52
				fcc(Ni)	10.86	39.40	49.74
				bcc(Cr)	2.10	93.26	4.64
A10	$Cu_{40.24}Cr_{46.00}Ni_{13.76}$	8	1000	fcc(Cu)	77.79	4.79	17.42
				fcc(Ni)	10.74	37.31	51.95
				bcc(Cr)	1.14	93.95	4.91
A11	$Cu_{84.38}Cr_{10.57}Ni_{5.05}$	8	1000	fcc(Cu)	91.37	1.85	6.78
				bcc(Cr)	2.92	95.04	2.04

Table 2
Phases and compositions of the Cu–Cr–Ag alloys annealed at 500, 600, 650 and 700 °C.

Alloy No.	Nominal composition (at.%)	Annealed time (days)	Annealed temperature (°C)	Phases identified by XRD and SEM/EDX	Composition (at.%)		
					Cu	Cr	Ag
B1	$Cu_{50}Cr_{40}Ag_{10}$	60	500	fcc(Ag)	10.46	2.67	86.87
				fcc(Cu)	96.36	1.90	1.74
				bcc(Cr)	1.79	98.14	0.07
B2	$Cu_{70}Cr_{20}Ag_{10}$	60	500	fcc(Ag)	10.03	2.55	87.42
				fcc(Cu)	96.57	1.20	2.23
				bcc(Cr)	3.20	96.44	0.36
B3	$Cu_2Cr_{10}Ag_{88}$	60	500	fcc(Ag)	4.40	0.99	94.61
				bcc(Cr)	0.72	97.98	1.30
B4	$Cu_{40}Cr_{40}Ag_{20}$	30	600	fcc(Ag)	10.90	1.95	87.15
				fcc(Cu)	97.30	0.96	1.74
				bcc(Cr)	1.98	97.95	0.07
B5	$Cu_{70}Cr_{10}Ag_{20}$	30	600	fcc(Cu)	96.91	0.94	2.15
				fcc(Ag)	11.14	1.97	86.89
				bcc(Cr)	3.02	96.85	0.13
B6	$Cu_2Cr_{10}Ag_{88}$	30	600	fcc(Ag)	6.27	1.25	92.48
				bcc(Cr)	0.47	96.58	2.95
B7	$Cu_{10}Cr_{10}Ag_{80}$	30	650	fcc(Cu)	96.39	0.49	3.12
				fcc(Ag)	11.92	1.49	86.59
				bcc(Cr)	0.61	98.71	0.68
B8	$Cu_{25}Cr_{10}Ag_{65}$	30	650	fcc(Cu)	96.66	0.67	2.67
				fcc(Ag)	13.46	0.77	85.77
				bcc(Cr)	1.58	98.06	0.36
B9	$Cu_{40}Cr_{10}Ag_{50}$	30	650	fcc(Cu)	96.84	0.64	2.52
				fcc(Ag)	12.65	1.57	85.78
				bcc(Cr)	2.20	97.07	0.73
B10	$Cu_{55}Cr_{10}Ag_{35}$	30	650	fcc(Cu)	96.98	0.62	2.40
				fcc(Ag)	12.22	1.07	86.71
				bcc(Cr)	4.13	95.40	0.47
B11	$Cu_{80}Cr_{10}Ag_{10}$	30	700	fcc(Cu)	95.80	0.74	3.46
				fcc(Ag)	17.06	2.35	80.59
				bcc(Cr)	3.48	96.15	0.37
B12	$Cu_{50}Cr_{10}Ag_{40}$	30	700	fcc(Cu)	92.29	4.37	3.34
				fcc(Ag)	15.84	1.02	83.14
				bcc(Cr)	2.28	97.22	0.50
B13	$Cu_5Cr_{10}Ag_{85}$	30	700	fcc(Ag)	11.33	1.17	87.50
				bcc(Cr)	1.68	88.87	9.45
B14	$Cu_{30}Cr_{40}Ag_{30}$	30	700	fcc(Cu)	95.33	1.26	3.41
				fcc(Ag)	13.37	1.14	85.49
				bcc(Cr)	1.84	97.75	0.41

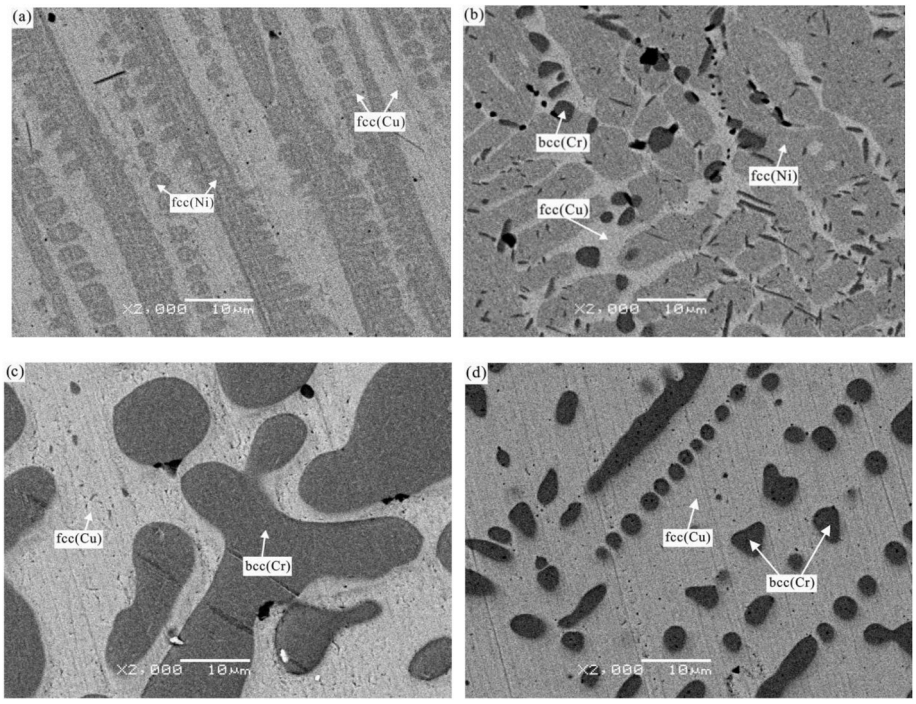

Fig. 2. The BSE micrographs of the Cu–Cr–Ni alloys at 800 °C annealed 15 days: (a) alloy A1 ($Cu_{54.15}Cr_{13.47}Ni_{32.38}$); (b) alloy A2 ($Cu_{29.15}Cr_{29.08}Ni_{41.77}$); (c) alloy A3 ($Cu_{55.79}Cr_{33.52}Ni_{10.69}$); (d) alloy A4 ($Cu_{76.97}Cr_{20.58}Ni_{2.45}$).

our constructed Cu alloys thermodynamic database [17]. In addition, many thermodynamic parameters of the fcc phase were used in the work of Ikoma and Kajihara [16]. For the Cu–Cr–Ag system, the microstructure and mechanical properties of the Cu–Cr–Ag alloys have been extensively studied [18–20]. However, no experimental data and thermodynamic description were available in the literature.

Thus, it is necessary to measure and assess the phase equilibria of the Cu–Cr–Ni and Cu–Cr–Ag systems. The purposes of the present work are to determine some representative isothermal sections of the Cu–Cr–Ni and Cu–Cr–Ag systems by key experiments including XRD and SEM/EDX, and to obtain a set of self-consistent thermodynamic parameters for the Cu–Cr–Ni and Cu–Cr–Ag systems by means of the CALPHAD approach [21,22].

2. Experimental procedures

The phase equilibria of the Cu–Cr–Ni system at 800 and 1000 °C, and the Cu–Cr–Ag system at 500, 600, 650 and 700 °C, were experimentally determined. Copper, chromium, nickel and silver rod with the purity of 99.99% (China New Metal Materials Technology Co., Ltd.) were used as raw materials. The nominal compositions of the alloys were shown in Fig. 1(a) and (b). 25 ternary alloys, each with a weight of approximately 1 g, were prepared in a non-consumable vacuum arc-melting furnace (WK–I, Physcience Opto-electronics Co., Ltd. Beijing, China) with water-cooled copper crucible under 99.999% pure Ar atmosphere. Each alloy was re-melted at least 5 times to improve their homogeneities. The alloys after arc melting were not subjected to chemical analysis since the weight losses were less than 1 wt. % for all alloys. Then the button samples were sealed in evacuated quartz capsules with vacuum sealing machine (MRVS-1002, Wuhan Bailibo Technology Co., Ltd., China), and annealed at 500 °C (60 days), 600 °C (30 days), 650 °C (30 days), 700 °C (30 days), 800 °C (15 or 20 days) and 1000 °C (8 days) in the high temperature diffusion furnace (KSL-1200X, Hefei Kejing Material Technology Co., Ltd., China), followed by quenching in cold water.

The XRD measurement of the annealed alloys was performed using a Cu-K_α radiation at 40 kV and 300 mA. Diffraction patterns were generally acquired in a scan step 0.02° of over a 2θ range 20–80°. Then the samples were further examined using scanning electron microscopy (SEM) equipped with energy dispersive X-ray analysis (EDX) (acceleration voltage 20 kV, scanning speed 10 μs, working distance 4.5 mm) (JSM-6360LV/GENESIS2000XM60, JEOL, Japan).

3. Thermodynamic model

The Gibbs energy functions of the pure elements Cu, Cr, Ni and Ag were taken from the SGTE database compiled by Dinsdale [23]. The thermodynamic parameters for the Cu–Cr [24], Cu–Ni [25], Cr–Ni [26], Cu–Ag [27] and Ag–Cr [28] systems were adopted in the present work. The calculated binary phase diagrams were presented in Fig. 1(a) and (b).

In the Cu–Cr–Ni and Cu–Cr–Ag systems, no binary and ternary phases exist. The solution phases, i.e. liquid, fcc and bcc, were described by the substitutional solution model. Taking the fcc phase as an example, its molar Gibbs energy of can be expressed by the Redlich-Kister-Muggianu polynomial [29]:

$$G_m^{fcc} = x_{Cu}\cdot {}^{\circ}G_{Cu}^{fcc} + x_{Cr}\cdot {}^{\circ}G_{Cr}^{fcc} + x_M\cdot {}^{\circ}G_M^{fcc} + R\cdot T\cdot(x_{Cu}\cdot \ln x_{Cu} + x_{Cr}\cdot \ln x_{Cr} + x_M\cdot \ln x_M) + x_{Cr}\cdot x_{Cu}\cdot L_{Cr,Cu}^{fcc} + x_{Cu}\cdot x_M\cdot L_{Cu,M}^{fcc} + x_{Cr}\cdot x_M\cdot L_{Cr,M}^{fcc} + {}^{ex}G^{fcc} \quad (1)$$

where R is the gas constant, T is temperature in Kelvin, x_{Cu}, x_{Cr} and x_M are the molar fractions of the elements Cu, Cr and M (M = Ni, Ag), respectively. The excess Gibbs energy ${}^{ex}G^{fcc}$ equals to $x_{Cr}\cdot x_{Cu}\cdot x_{Ni}\cdot(x_{Cr}\cdot {}^{0}L_{Cr,Cu,Ni}^{fcc} + x_{Cu}\cdot {}^{1}L_{Cr,Cu,Ni}^{fcc} + x_{Ni}\cdot {}^{2}L_{Cr,Cu,Ni}^{fcc})$ in the Cu–Cr–Ni system or $x_{Ag}\cdot x_{Cr}\cdot x_{Cu}\cdot(x_{Ag}\cdot {}^{0}L_{Ag,Cr,Cu}^{fcc} + x_{Cr}\cdot {}^{1}L_{Ag,Cr,Cu}^{fcc} + x_{Cu}\cdot {}^{2}L_{Ag,Cr,Cu}^{fcc})$ in the Cu–Cr–Ag system, respectively. The ternary interaction parameters ${}^{0}L^{fcc}$, ${}^{1}L^{fcc}$ and ${}^{2}L^{fcc}$ are linearly temperature-dependent, which can be expressed as $L^{fcc} = A + B\cdot T$. The coefficients A and B were optimized

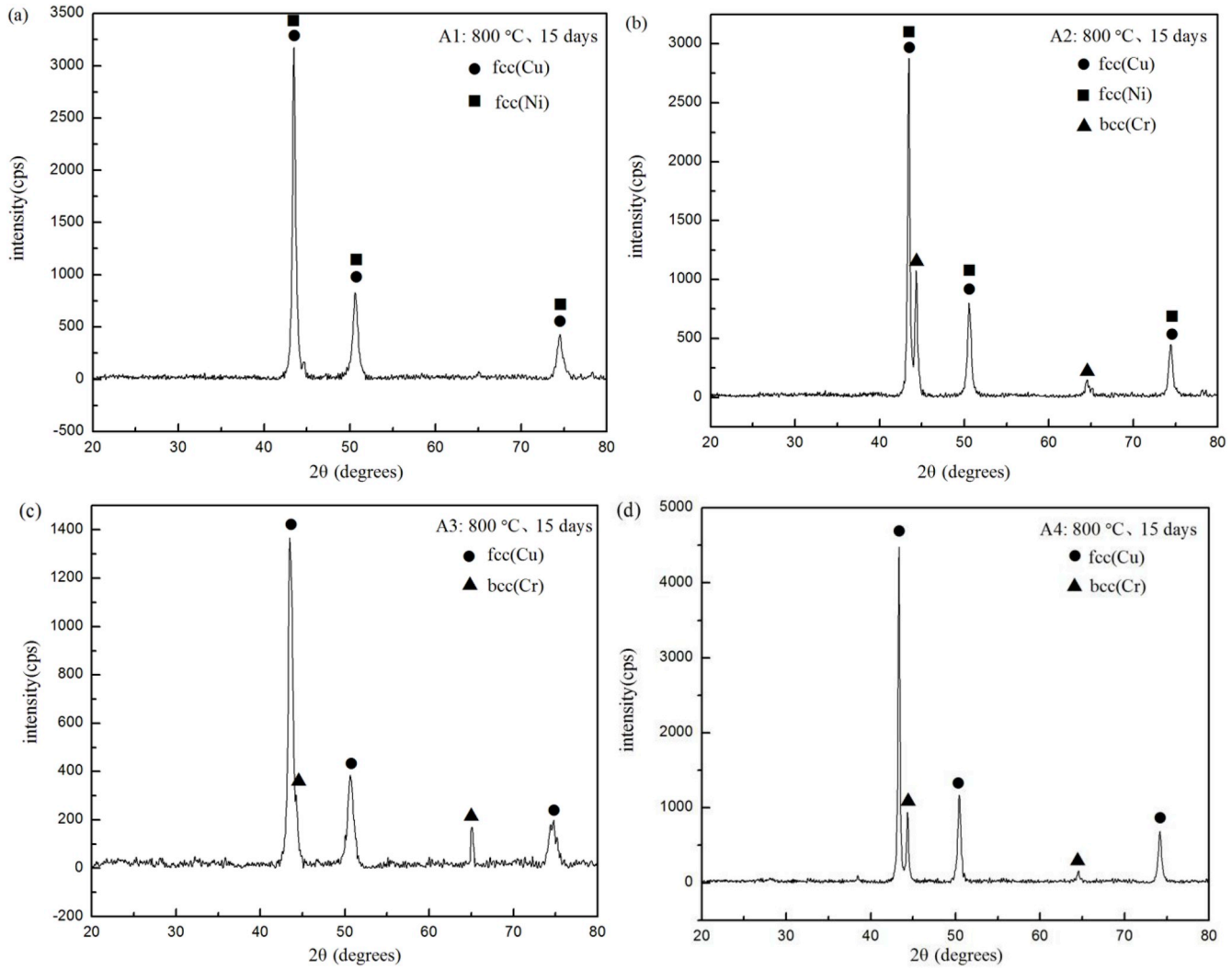

Fig. 3. XRD patterns of the Cu–Cr–Ni alloys at 800 °C annealed 15 days: (a) alloy A1 ($Cu_{54.15}Cr_{13.47}Ni_{32.38}$); (b) alloy A2 ($Cu_{29.15}Cr_{29.08}Ni_{41.77}$); (c) alloy A3 ($Cu_{55.79}Cr_{33.52}Ni_{10.69}$); (d) alloy A4 ($Cu_{76.97}Cr_{20.58}Ni_{2.45}$).

according to the experimental data available from the literature and present work.

4. Results and discussion

4.1. Experimental results and discussion

Eleven and fourteen alloys were prepared to determine the phase equilibria of the Cu–Cr–Ni system at 800 and 1000 °C, and the Cu–Cr–Ag system at 500, 600, 650 and 700 °C, respectively. The phases were identified by XRD and the composition and microstructure were measured by SEM/DEX. The experimental results are listed in Tables 1 and 2.

Alloys A1-A7 were prepared for determining the isothermal section of the Cu–Cr–Ni system at 800 °C. Figs. 2 and 3 show the backscattered electron (BSE) images and XRD patterns of the A1-A4 alloys annealed at 800 °C for 15 days, respectively. Figs. 2 (a) and Fig. 3 (a) are the BSE micrograph and XRD patterns for the alloy A1 ($Cu_{54.15}Cr_{13.47}Ni_{32.38}$), respectively. According to the SEM/EDX measurement results, there are two phases in equilibrium of the A1 alloys, one phase in the Cu-rich region, and the other one in the Ni-rich region. Combined with the XRD results, the A1 alloy located in a two-phase region light gray fcc(Cu) and dark gray fcc(Ni). The XRD patterns of the fcc(Cu) phase overlap that of the fcc(Ni) phase due to the same crystal structure face-centered cubic (fcc). This phase region is the fcc miscibility gap. Similarly, the phases of the A2-A7 alloys are also determined. The alloy A2 ($Cu_{29.15}Cr_{29.08}Ni_{41.77}$) is located in a three-phase region, i.e. light gray fcc(Cu), dark gray fcc(Ni), and the black bcc(Cr) (see Fig. 2 (b) and 3 (b)). For both alloys A3 ($Cu_{55.79}Cr_{33.52}Ni_{10.69}$) and A4 ($Cu_{76.97}Cr_{20.58}Ni_{2.45}$), two phases fcc(Cu) and bcc(Cr) coexist (see Fig. 2 (c) and (d), and Fig. 3 (c) and (d)). Alloys A5 ($Cu_{31.50}Cr_{15.70}Ni_{52.80}$) and A6 ($Cu_{36.40}Cr_{21.80}Ni_{41.80}$) are in a two-phase region, i.e. fcc(Cu) + fcc (Ni), and alloy A7 ($Cu_{40.70}Cr_{26.80}Ni_{32.50}$) is in a three-phase region, i.e. fcc(Cu) + fcc(Ni) + bcc(Cr). It is concluded that one three-phase region fcc(Cu) + fcc(Ni) + bcc(Cr), and two two-phase regions fcc(Cu) + fcc (Ni) and fcc(Cu) + bcc(Cr) are determined. No ternary compound is found in the present work. The measured maximum solubility of Cr in the fcc(Cu) phase is about 4 at.%. The solubilities of Cu and Ni in the bcc (Cr) phase are about 3 at.%. fcc(Ni) has a large single-phase region with the solubilities of 30 at.% Cu and 17 at.% Cr. The isothermal section of the Cu–Cr–Ni system at 800 °C determined by the present work is similar with the experimental results reported by Ikoma [15].

In order to measure the phase equilibria of the Cu–Cr–Ni system at 1000 °C, four alloys A8-A11 were prepared in the present work. Figs. 4 and 5 show the backscattered electron (BSE) images and XRD patterns of the A8-A11 alloys annealed at 1000 °C for 8 days, respectively.

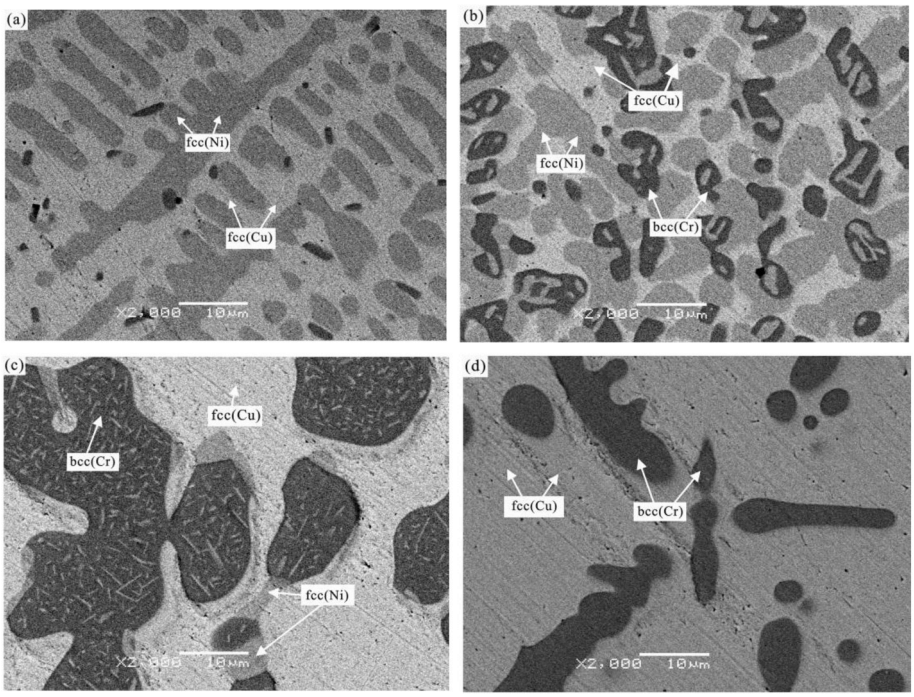

Fig. 4. The BSE micrographs of the Cu–Cr–Ni alloys at 1000 °C annealed 8 days: (a) alloy A8 ($Cu_{47.35}Cr_{20.29}Ni_{32.36}$); (b) alloy A9 ($Cu_{27.06}Cr_{40.57}Ni_{32.37}$); (c) alloy A10 ($Cu_{40.24}Cr_{46.00}Ni_{13.76}$); (d) alloy A11 ($Cu_{84.38}Cr_{10.57}Ni_{5.05}$).

Combined with the SEM/EDX and XRD measured results, the phases of the A8-A11 alloys are analyzed. The alloys A8 ($Cu_{47.35}Cr_{20.29}Ni_{32.36}$) and A11 ($Cu_{84.38}Cr_{10.57}Ni_{5.05}$) are located in a two-phase region, i.e. fcc (Cu) + fcc(Ni) and fcc(Cu) + bcc(Cr), respectively. The alloys A9 ($Cu_{27.06}Cr_{40.57}Ni_{32.37}$) and A10 ($Cu_{40.24}Cr_{46.00}Ni_{13.76}$) are located the same three-phase region fcc(Cu) + fcc(Ni) + bcc(Cr). The phase equilibria of the Cu–Cr–Ni system at 1000 °C are the similar with the ones at 800 °C. The fcc(Ni) single-phase region at 1000 °C is larger than the one at 800 °C. The measured solubility of Cr in the fcc(Cu) phase is about 4 at.% and the solubilities of Cu and Ni in the bcc(Cr) phase are less than 5 at.%.

Alloys B1–B14 are prepared for determining the isothermal sections of the Cu–Cr–Ag system at 500, 600, 650 and 700 °C. Combined with the SEM/EDX and XRD measured results, the phases and compositions of the B1–B14 alloys are analyzed and listed in Table 2. Figs. 6 and 7 show the backscattered electron (BSE) images and XRD patterns of some representative alloys annealed at 500 °C (60 days), 600 °C (30 days), 650 °C (30 days) and 700 °C (30 days), respectively. As indicated in these figures, the alloys B1 ($Cu_{50}Cr_{40}Ag_{10}$), B4 ($Cu_{40}Cr_{40}Ag_{20}$), B7 ($Cu_{10}Cr_{10}Ag_{80}$), B10 ($Cu_{55}Cr_{10}Ag_{35}$) and B14 ($Cu_{30}Cr_{40}Ag_{30}$) are located in the same three-phase region fcc(Cu) + fcc(Ag) + bcc(Cr). The alloys B3 ($Cu_2Cr_{10}Ag_{88}$), B6 ($Cu_2Cr_{10}Ag_{88}$) and B13 ($Cu_5Cr_{10}Ag_{85}$) are located the same two-phase region fcc(Ag) + bcc(Cr). The measured phase equilibria of the Cu–Cr–Ag system are simple and similar at 500, 600, 650 and 700 °C. No ternary compound is found in the Cu–Cr–Ag system. The measured solubility of Cu in the fcc(Ag) phase is about 10, 11 12.5, 17 at.% at 500, 600, 650 and 700 °C, respectively. The solubilities of Cr in the fcc(Ag) phase, Cu and Ag in the bcc(Cr) phase, Ag and Cr in the fcc (Cu) phase are all limited to be about 2 at.%.

4.2. Thermodynamic calculation results and discussion

Based on the experimental data available in present work and the literature, the Cu–Cr–Ni and Cu–Cr–Ag systems were evaluated by the optimization module PARROT [30] of the program Thermo-Calc, which works by minimizing the square sum of the differences between measured and calculated values. The obtained thermodynamic parameters of the Cu–Cr–Ni and Cu–Cr–Ag systems were listed in Table 3. Some representative phase diagrams of the Cu–Cr–Ni and Cu–Cr–Ag systems were calculated.

Fig. 8 (a) and (b) show the calculated isothermal sections of the Cu–Cr–Ni system at 800 and 1000 °C, respectively, along with the experimental data obtained in the present work and reported by Ikoma [15]. As can be seen from the two isothermal sections, most of the experimental data can be well reproduced by the present calculations. In addition, the calculated results are consistent with the calculated one from Ikoma and Kajihara [16]. However, fewer ternary parameters of the fcc phase are used in the present work. It is conducive to extrapolation to high-order systems.

Fig. 8 (c) shows the calculated isothermal section at 930 °C of the Cu–Cr–Ni system along with the experimental data from Meijering et al. [13]. According to the experimental and calculated results as shown in Fig. 8 (a) and (b), the fcc(Ni) region increases with the increase of temperature from 800 to 1000 °C and the composition of fcc(Ni) in the three-phase region fcc(Ni) + fcc(Cu) + bcc(Cr) moves towards the Cu–Cr boundary. However, the region of the fcc(Ni) reported by Meijering et al. [13] at 930 °C is smaller than 800 °C and the composition of fcc(Ni) in the three-phase region fcc(Ni) + fcc(Cu) + bcc(Cr) is higher than the one determined in the present work and in the work of Ikoma [15]. In addition, the phase composition was not determined by SEM/EDX according to the work of Meijering et al. [13]. The composition of the three-phase region fcc(Ni) + fcc(Cu) + bcc(Cr) reported by Meijering et al. [13] is questionable. Thus, the piece of experimental data from Meijering et al. [13] is not used in the optimization and only shown for comparison.

Fig. 9 presents the calculated isothermal sections of the Cu–Cr–Ag system at 500, 600, 650 and 700 °C along with the experimental data obtained in the present work. As can be seen from the four isothermal sections, most of the experimental data can be well reproduced by the present calculations. The calculated solubilities of Cu in the fcc(Ag) phase to be about 5 and 7 at.% at 500 and 600 °C, respectively, are a little less than the measured ones 10 and 11 at.%. Due to the limited

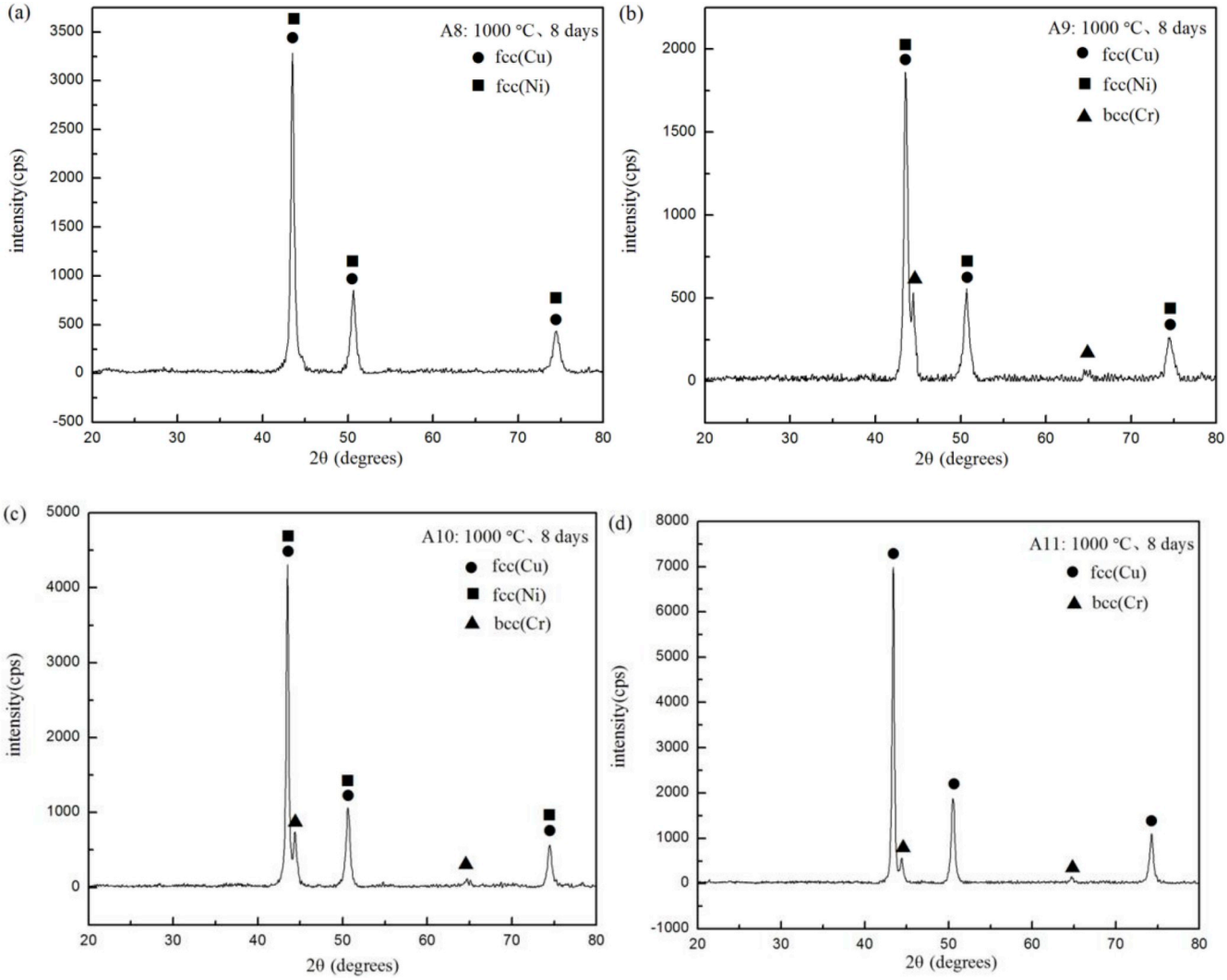

Fig. 5. XRD patterns of the Cu–Cr–Ni alloys at 1000 °C annealed 8 days: (a) alloy A8 ($Cu_{47.35}Cr_{20.29}Ni_{32.36}$); (b) alloy A9 ($Cu_{27.06}Cr_{40.57}Ni_{32.37}$); (c) alloy A10 ($Cu_{40.24}Cr_{46.00}Ni_{13.76}$); (d) alloy A11 ($Cu_{84.38}Cr_{10.57}Ni_{5.05}$).

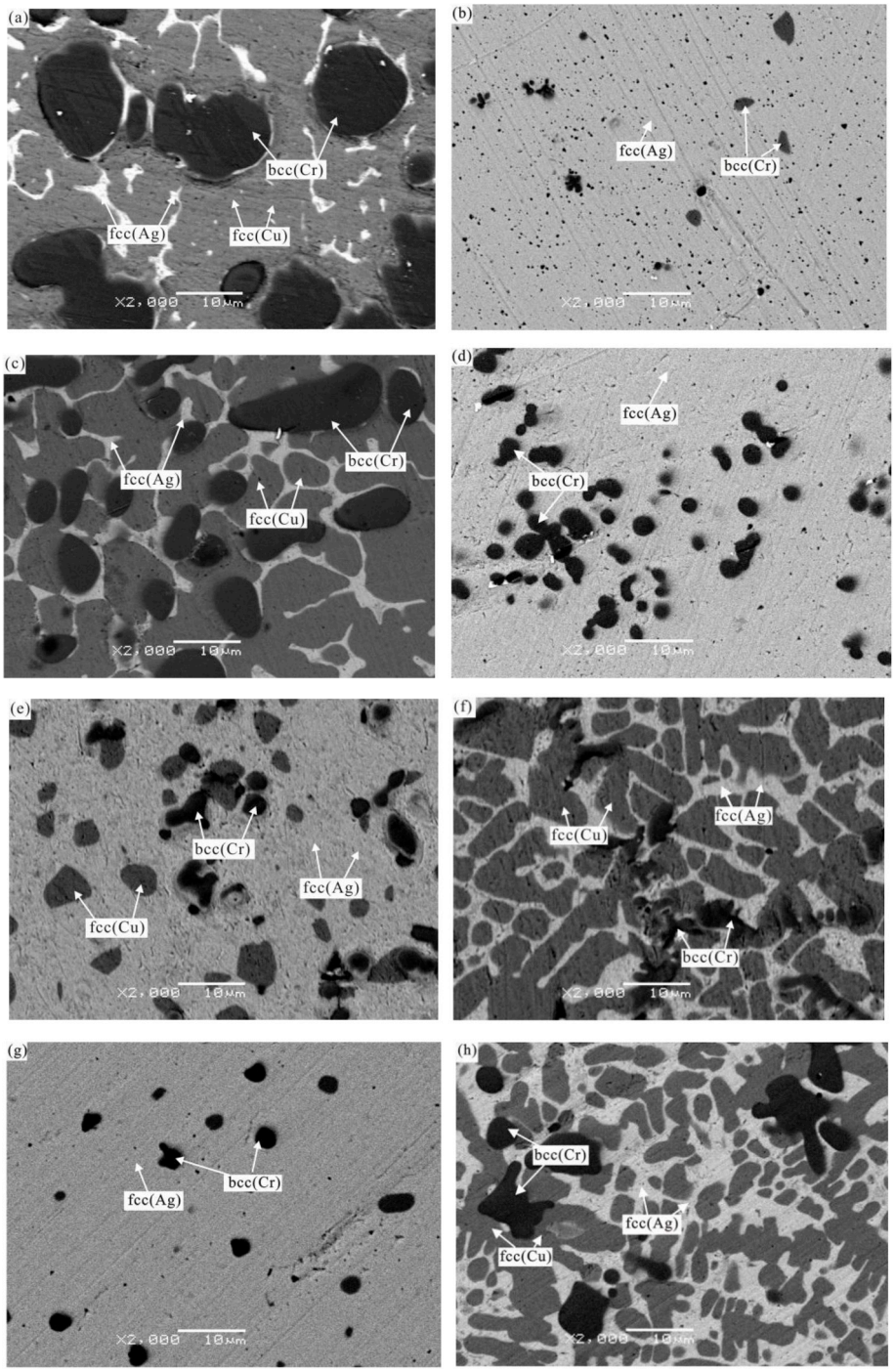

Fig. 6. The BSE micrographs of the Cu–Cr–Ag alloys annealed at 500 °C (60 days), 600 °C (30 days), 650 °C (30 days), and 700 °C (30 days): (a) alloy B1 ($Cu_{50}Cr_{40}Ag_{10}$); (b) alloy B3 ($Cu_2Cr_{10}Ag_{88}$); (c) alloy B4 ($Cu_{40}Cr_{40}Ag_{20}$); (d) alloy B6 ($Cu_2Cr_{10}Ag_{88}$); (e) alloy B7 ($Cu_{10}Cr_{10}Ag_{80}$); (f) alloy B10 ($Cu_{55}Cr_{10}Ag_{35}$); (g) alloy B13 ($Cu_5Cr_{10}Ag_{85}$); (h) alloy B14 ($Cu_{30}Cr_{40}Ag_{30}$).

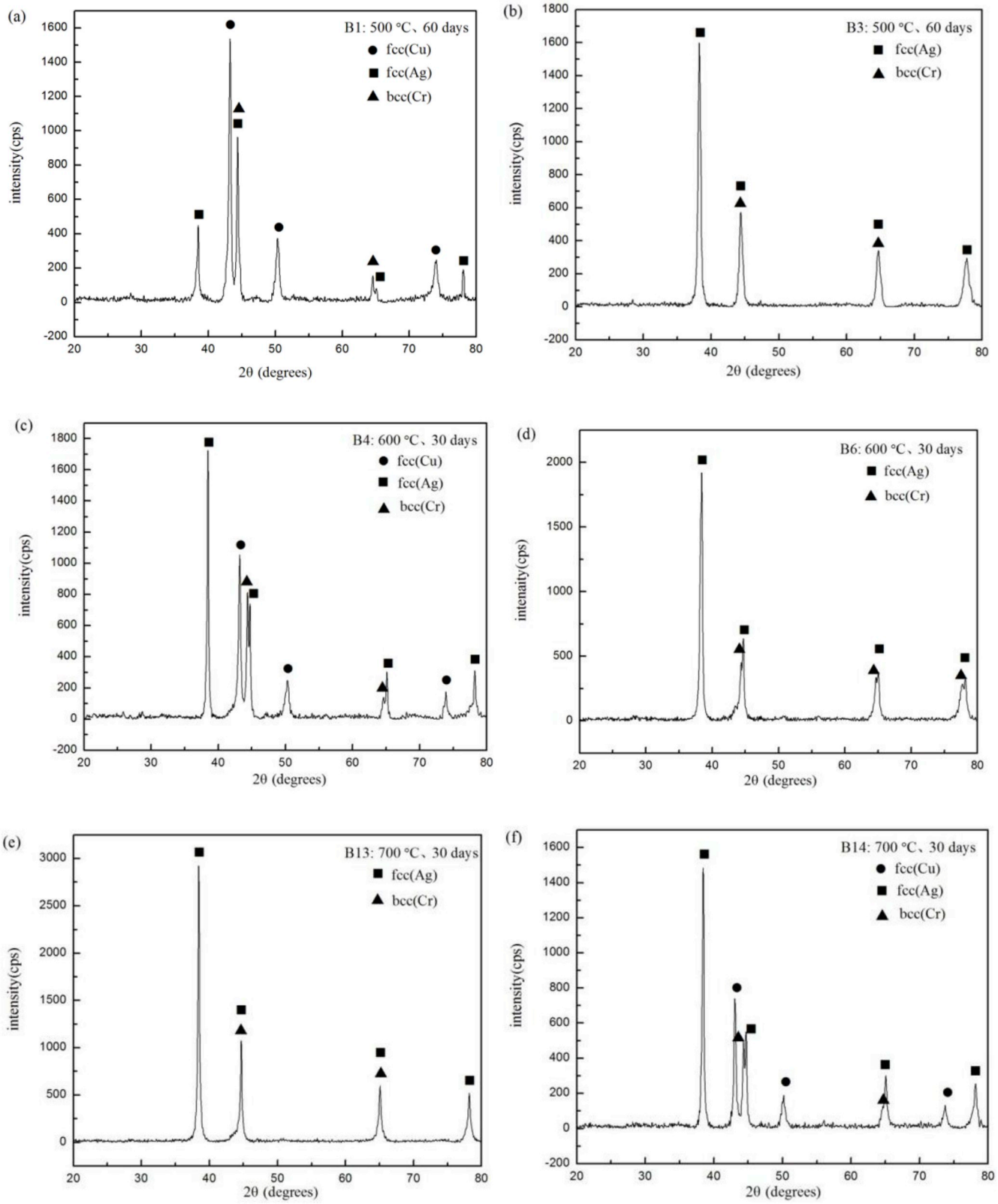

Fig. 7. XRD patterns of the Cu–Cr–Ni alloys annealed at 500 °C (60 days), 600 °C (30 days), and 700 °C (30 days): (a) alloy B1 ($Cu_{50}Cr_{40}Ag_{10}$); (b) alloy B3 ($Cu_2Cr_{10}Ag_{88}$); (c) alloy B4 ($Cu_{40}Cr_{40}Ag_{20}$); (d) alloy B6 ($Cu_2Cr_{10}Ag_{88}$); (e) alloy B13 ($Cu_5Cr_{10}Ag_{85}$); (f) alloy B14 ($Cu_{30}Cr_{40}Ag_{30}$).

Table 3
Summary of the thermodynamic parameters in the Cu–Cr–Ni and Cu–Cr–Ag systems[a].

System	Phases/Models	Thermodynamic parameters	Reference
Cu–Cr–Ni	liquid: (Cr, Cu, Ni)$_1$	${}^0L^{liquid}_{Cr,Cu} = 38795.8 - 3.68{\cdot}T$	[24]
		${}^1L^{liquid}_{Cr,Cu} = 3760 - 2.62{\cdot}T$	[24]
		${}^2L^{liquid}_{Cr,Cu} = 44731.3 - 21.05{\cdot}T$	[24]
		${}^0L^{liquid}_{Cu,Ni} = 12048.61 - 1.3{\cdot}T$	[25]
		${}^1L^{liquid}_{Cu,Ni} = -1861.61 + 0.94{\cdot}T$	[25]
		${}^0L^{liquid}_{Cr,Ni} = 318 - 7.3318{\cdot}T$	[26]
		${}^1L^{liquid}_{Cr,Ni} = 16941 - 6.3696{\cdot}T$	[26]
	fcc_A1: (Cr, Cu, Ni)$_1$Va$_1$	${}^0L^{fcc\_A1}_{Cr,Cu:Va} = 52900$	[24]
		${}^0L^{fcc\_A1}_{Cu,Ni:Va} = -2041.3 + T$	[25]
		${}^0L^{fcc\_A1}_{Cr,Ni:Va} = 8030 - 12.8801{\cdot}T$	[26]
		${}^1L^{fcc\_A1}_{Cr,Ni:Va} = 33080 - 16.0362{\cdot}T$	[26]
		${}^0L^{fcc\_A1}_{Cr,Cu,Ni:Va} = -60633$	This wok
		${}^1L^{fcc\_A1}_{Cr,Cu,Ni:Va} = -262801 + 175{\cdot}T$	This wok
	bcc_A2: (Cr, Cu, Ni)$_1$Va$_3$	${}^0L^{bcc\_A2}_{Cr,Cu:Va} = 81000$	[24]
		${}^0L^{bcc\_A2}_{Cu,Ni:Va} = 8047.72 + 3.442217{\cdot}T$	[25]
		${}^1L^{bcc\_A2}_{Cu,Ni:Va} = 2041.3 + 0.99714{\cdot}T$	[25]
		${}^0L^{bcc\_A2}_{Cr,Ni:Va} = 17170 - 11.8199{\cdot}T$	[26]
		${}^1L^{bcc\_A2}_{Cu,Ni:Va} = 34418 - 118577{\cdot}T$	[26]
Cu–Cr–Ag	liquid: (Ag, Cr, Cu)$_1$	${}^1L^{liquid}_{Cr,Cu} = 38795.8 - 3.68{\cdot}T$	[24]
		${}^1L^{liquid}_{Cr,Cu} = 3760 + 2.62{\cdot}T$	[24]
		${}^1L^{liquid}_{Cr,Cu} = 44731.3 - 21.05{\cdot}T$	[24]
		${}^0L^{liquid}_{Ag,Cu} = 16914.949 - 14.7721{\cdot}T + 1.54955{\cdot}T{\cdot}\ln(T)$	[27]
		$L^{liquid}_{Ag,Cu} = -1963.3 + 0.8623{\cdot}T$	[27]
		${}^0L^{liquid}_{Ag,Cr} = 2194716$	[28]
		${}^1L^{liquid}_{Ag,Cr} = 2446830$	[28]
		${}^2L^{liquid}_{Ag,Cr} = 14332$	[28]
	fcc_A1: (Ag, Cr, Cu)$_1$Va$_1$	${}^0L^{fcc\_A1}_{Cr,Cu:Va} = 52900$	[24]
		${}^0L^{fcc\_A1}_{Ag,Cu:Va} = 32580.365 - 7.4547{\cdot}T$	[27]
		${}^1L^{fcc\_A1}_{Ag,Cu:Va} = -10144.596 + 5.562{\cdot}T$	[27]
		${}^0L^{fcc\_A1}_{Ag,Cr:Va} = 69838$	[28]
		${}^0L^{fcc\_A1}_{Ag,Cr,Cu:Va} = -338000$	This work
	bcc_A2: (Ag, Cr, Cu)$_1$Va$_3$	${}^0L^{bcc\_A2}_{Cr,Cu:Va} = 81000$	[24]
		${}^0L^{bcc\_A2}_{Ag,Cu:Va} = 12000$	[27]
		${}^0L^{bcc\_A2}_{Ag,Cr:Va} = 338594$	[28]

[a] Temperature (T) in Kelvin and Gibbs energy in J/mol-atom. The Gibbs energies for the pure elements are taken from the compilation of Dinsdale [23]. The thermodynamic parameters for the Cu-Cr [24], Cu-Ni [25], Cr-Ni [26], Cu-Ag [27] and Ag–Cr [28] systems are adopted in the present work.

region of the fcc(Ag) phase, it is difficult to completely reproduce the solubilities of the fcc(Ag) phase at 500 and 600 °C in the present modeling. Considering the experimental error, the present calculations are acceptable.

5. Conclusions

The isothermal sections of the Cu–Cr–Ni system at 800 and 1000 °C, and Cu–Cr–Ag system at 500, 600, 650 and 700 °C, were investigated by means of the XRD and SEM methods. One three-phase region fcc(Cu) + bcc(Cr) + fcc(Ni) and two two-phase regions fcc(Cu) + fcc(Ni) and fcc (Cu) + bcc(Cr) in the Cu–Cr–Ni system, and one three-phase region fcc (Cu) + bcc(Cr) + fcc(Ag) and one two-phase region fcc(Ag) + bcc(Cr) in the Cu–Cr–Ag system were determined. No ternary compound was found in the two ternary systems.

The thermodynamic assessment of the Cu–Cr–Ni and Cu–Cr–Ag systems was performed by the CALPHAD method based on the experimental phase equilibria data available in the present work and the literatures. A set of self-consistent thermodynamic parameters of the Cu–Cr–Ni and Cu–Cr–Ag systems was obtained. Most of the reliable experimental data can be well reproduced by the present thermodynamic modeling.

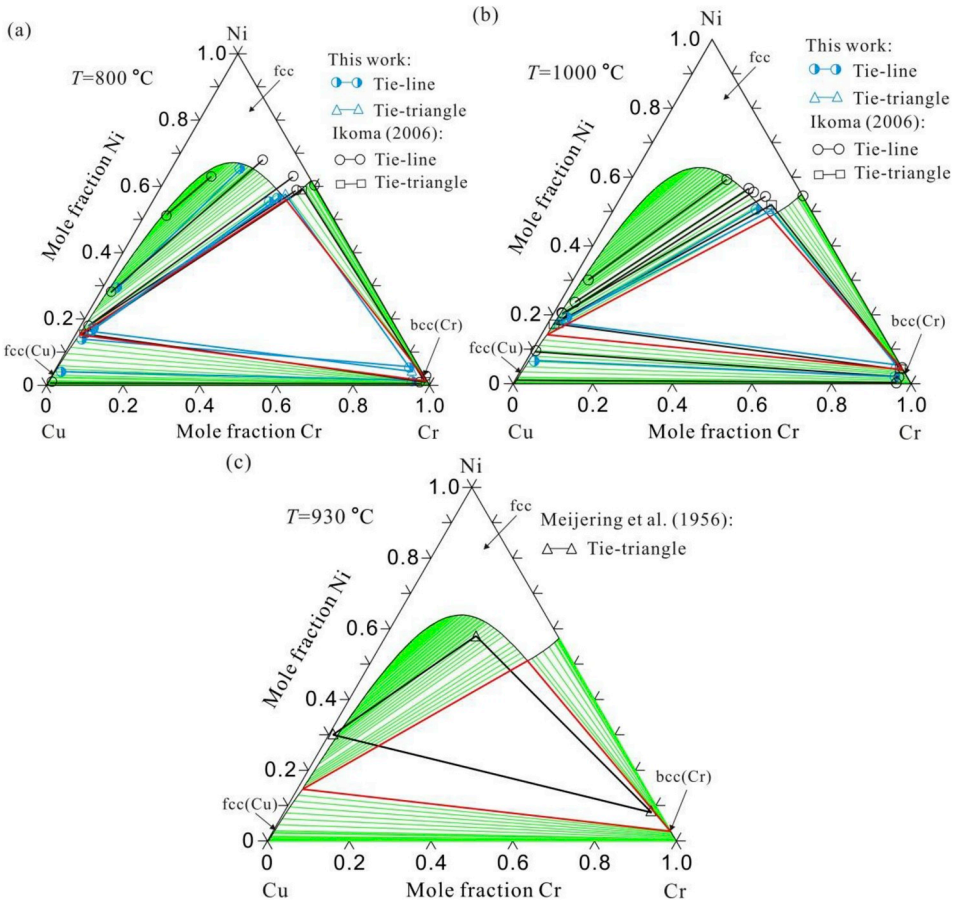

Fig. 8. Calculated isothermal sections of the Cu–Cr–Ni system along with the experimental data from the present work and literature [15]: (a) 800 °C; (b) 1000 °C; (c) 930 °C.

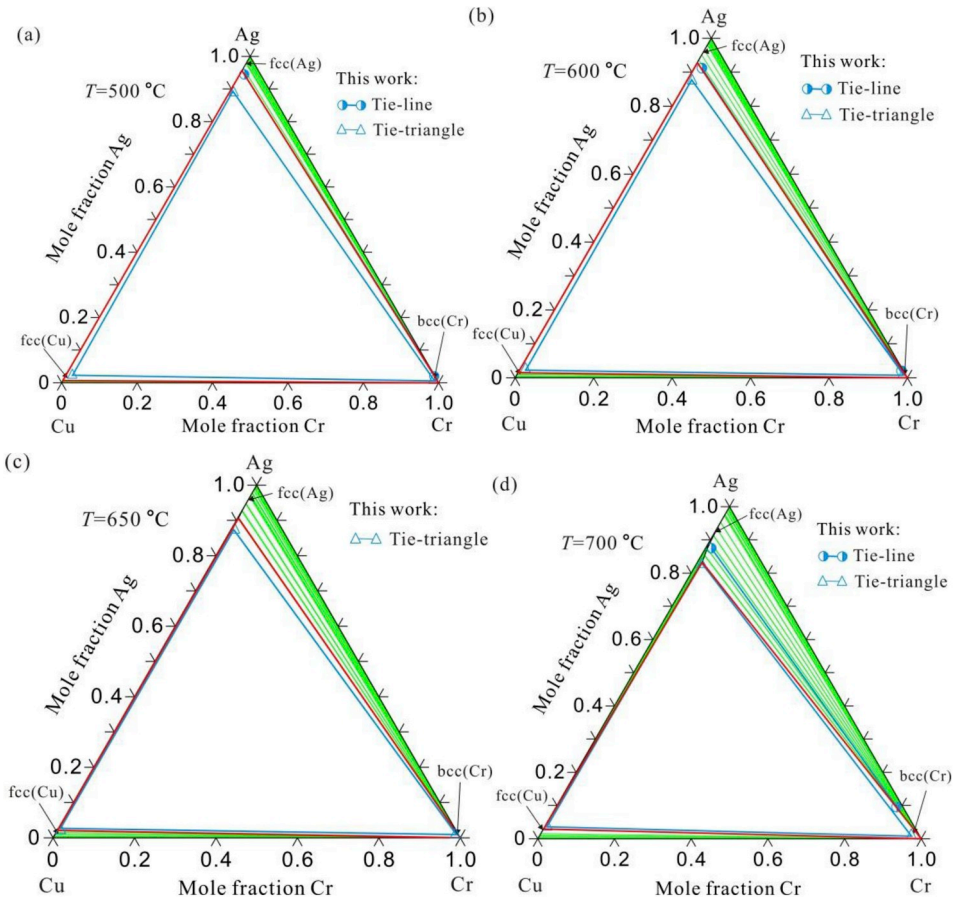

Fig. 9. Calculated isothermal sections of the Cu–Cr–Ag system along with the experimental data from the present work: (a) 500 °C; (b) 600 °C; (c) 650 °C; (d) 700 °C.

Declaration of competing interest

The authors declared that there are no conflicts of interest for this work.

Acknowledgements

The financial support from Anhui Province University Natural Science Research Projects of China (No. KJ2019A0113), Key Research and Development Plan Projection of Anhui Province of China (No. 201904a05020092), Anhui Province Postdoctoral Science Foundation of China (No. 2017B210) and National Undergraduate Innovation and Entrepreneurship Training Program in 2019 are greatly acknowledged.

Appendix A. Supplementary data

Supplementary data to this article can be found online at https://doi.org/10.1016/j.calphad.2019.101734.

References

[1] A.H. Huang, Y.F. Wang, M.S. Wang, L.Y. Song, Y.S. Li, L. Gao, C.X. Huang, Y. T. Zhu, Optimizing the strength, ductility and electrical conductivity of a Cu-Cr-Zr alloy by rotary swaging and aging treatment, Mater. Sci. Eng. A 746 (2019) 211–216.
[2] Y.X. Zhao, T.K. Pang, J.X. He, X.M. Tao, H.M. Chen, Y.F. Ouyang, Y. Du, Interdiffusion behaviors and mechanical properties of Cu-Zr system, Calphad 61 (2018) 92–97.
[3] X.S. Zhang, Y.J. Chen, J.L. Hu, Recent advances in the development of aerospace materials, Prog. Aerosp. Sci. 97 (2018) 22–34.
[4] F. Wang, K. von Klinski-Wetzel, R. Mukherjee, B. Nestler, M. Heilmaier, Experimental and numerical investigation on the phase separation affected by cooling rates and marangoni convection in Cu-Cr alloys, Metall. Mater. Trans. A 46 (2015) 1756–1766.
[5] D. Shangina, Y. Maksimenkova, N. Bochvar, V. Serebryany, G. Raab, A. Vinogradov, W. Skrotzki, S. Dobatkin, Influence of alloying with hafnium on the microstructure, texture, and properties of Cu-Cr alloy after equal channel angular pressing, J. Mater. Sci. 51 (2016) 5493–5501.
[6] Y. Zhang, S. Huili, A.A. Volinsky, B.H. Tian, Z. Chai, P. Liu, Y. Liu, Hot deformation and dynamic recrystallization behavior of the Cu-Cr-Zr-Y alloy, J. Mater. Eng. Perform. 25 (2016) 1150–1156.
[7] Y.L. Liu, P. Zhou, S.H. Liu, Y. Du, Experimental investigation and thermodynamic description of the Cu-Cr-Zr system, Calphad 59 (2017) 1–11.
[8] G.L. Xu, L.J. Peng, G.J. Huang, H.F. Xie, Z. Yang, X. Feng, X.Q. Yin, X.J. Mi, Microstructural evolution and properties of a Cu-Cr-Ag alloy during continuous manufacturing process, Rare Met. 38 (2019) 1–11.
[9] S. Xu, H.D. Fu, Y.T. Wang, J.X. Xie, Effect of Ag addition on the microstructure and mechanical properties of Cu-Cr alloy, Mater. Sci. Eng. A 726 (2018) 208–214.
[10] H. Chen, P. Gao, H. Peng, H. Wei, W. Xie, H. Wang, B. Yang, Study on the hot deformation behavior and microstructure evolution of Cu-Cr-In alloy, Mater. Eng. Perform. 28 (2019) 2128–2136.
[11] C. Kim, B. Lim, B. Kim, U. Shim, S. Oh, B. Sung, J. Choi, J. Ki, S. Baik, Strengthening of copper matrix composites by nickel-coated single-walled carbon nanotube reinforcements, Synth. Met. 159 (2009) 424–429.
[12] C. Watanabe, R. Monzen, K. Tazaki, Mechanical properties of Cu-Cr system alloys with and without Zr and Ag, J. Mater. Sci. 43 (2008) 813–819.
[13] J.L. Meijering, G.W. Rathenau, M.G. Vandersteeg, P.B. Braun, A miscibility gap in the face-centred cubic phase of the copper-nickel-chromium system, J. Inst. Metals 84 (1955-1956) 118–120.
[14] J.L. Meijering, Calculation of the nickel-chromium-copper phase diagram from binary data, Acta Metall. 5 (1957) 257–264.
[15] T. Ikoma, Mater. Eng, Ph.D. thesis, Tokyo Institute of Technology, Tokyo, 2006.
[16] T. Ikoma, M. Kajihara, Thermodynamic evaluation of phase equilibria in the ternary Cu-Cr-Ni system, Mater. Sci. Eng. A 437 (2006) 293–300.
[17] B. Hu, Y. Du, S.H. Liu, Y.L. Liu, L. Huang, C.Y. Shi, A new thermodynamic database for multicomponent Cu alloys, in: R. Arróyave (Ed.), An Overview of CALPHAD XLVII (Juriquilla, Querétaro, México), Calphad, vol. 67, 2019, p. 101618.
[18] S.G. Jia, M.S. Zheng, P. Liu, F.Z. Ren, B.H. Tian, G.S. Zhou, H.F. Lou, Aging properties studies in a Cu-Ag-Cr alloy, Mater. Sci. Eng. A 419 (2006) 8–11.
[19] S.G. Jia, P. Liu, F.Z. Ren, B.H. Tian, M.S. Zheng, G.S. Zhou, Electrotribological property of the Cu-Ag-Cr alloy with high-strength and high-conductivity, Met. Mater. Int. 13 (2007) 25–30.
[20] D.W. Yuan, B. Yang, J.S. Chen, H.M. Chen, J.B. Zhang, H. Wang, Upward continuous casting in the manufacture of Cu-Cr-Ag alloys: potential for enhancing

strength whilst maintaining ductility, Metall. Mater. Trans. A 48 (2017) 6083–6090.
[21] Z.K. Liu, Y. Wang, Computational Thermodynamics of Materials, Cambridge University Press, Cambridge, 2016.
[22] H. Lukas, S.G. Fries, B. Sundman, Computational Thermodynamics: the CALPHAD Method, Cambridge University Press, Cambridge, 2007.
[23] A.T. Dinsdale, SGTE data for pure elements, Calphad 15 (1991) 317–425.
[24] K.J. Zeng, M. Hamalainena, Thermodynamic analysis of stable and metastable equilibria in the Cu-Cr system, Calphad 19 (1995) 93–104.
[25] S. an Mey, Thermodynamic re-evaluation of the Cu-Ni system, Calphad 16 (1992) 255–260.
[26] B.J. Lee, On the stability of Cr carbides, Calphad 16 (1992) 121–149.
[27] X.C. He, H. Wang, H.S. Liu, Z.P. Jin, Thermodynamic description of the Cu-Ag-Zr system, Calphad 30 (2006) 367–374.
[28] Y.B. Peng, Yong Du, Unpubilshed Work, 2011.
[29] O. Redlich, A.T. Kister, Thermodynamics of nonelectrolyte solutions, Ind. Eng. Chem. 40 (1948) 345–348.
[30] B. Sundman, B. Jansson, J.O. Andersson, The thermo-calc databank system, Calphad 9 (1985) 153–190.